Excited States of 1,6-Methano[10]annulene: Site Selection Fluorescence and Fluorescence Excitation Spectroscopy on S_1

Lorenzo Catani, Cristina Gellini, and Pier Remigio Salvi*

Laboratorio di Spettroscopia Molecolare, Dipartimento di Chimica, Università di Firenze, Via G. Capponi 9, 50121 Firenze, Italy

Received: November 11, 1997; In Final Form: December 30, 1997

Fluorescence, $S_1 \rightarrow S_0$, and fluorescence excitation, $S_0 \rightarrow S_1$, spectra of 1,6-methano[10]annulene have been measured in glassy matrixes at low temperature under moderate site selection conditions. The polarization ratios of both spectra have been also measured at 77 K. MO ab initio calculations including correlation effects indicate that the molecule has one energy minimum in the ground state and one in the lowest excited singlet state. They correspond to bond-equalized structures of aromatic character. The spectra are accordingly discussed in terms of transitions involving the aromatic form of 1,6-methano[10]annulene. A good correlation is found between observed and calculated Franck−Condon intensities.

I. Introduction

The lowest excited states of aromatic molecules have been thouroughly investigated by means of electronic spectroscopy for a long time.[1] The large amount of spectroscopic data available on simple aromatics (benzene, naphthalene, anthracene, etc., and derivatives) have played a major role in the study of excited-state structure and properties[1,2] and in modeling theories in different fields of chemical research.[3−6]

The one-photon spectrum of these molecules in the low-energy region has been interpreted in a first approximation as due to electronic promotions between the two highest occupied π and the two lowest virtual π^* molecular orbitals. These give rise to the well-known L_b, L_a, B_b, and B_a transitions in Platt's nomenclature.[7] One- and two-photon L_b spectra show well-resolved vibronic structures under a large variety of experimental conditions[8−13] and may be taken as prototype examples of absorption strength originating from interaction between electronic states,[14−17] the L_b transition being forbidden in the two-photon and only weakly allowed (or forbidden, in the benzene case) in one-photon spectroscopy.

Equivalent information[18] is not available for higher homologues of benzene, i.e., [4*n*+2]annulenes with $n \geq 2$. The next higher, potentially aromatic, homologue of benzene is [10]-annulene, which may exist in three configurations, all-cis,[19] mono-trans,[19] and trans−trans. For steric reasons (ring strain or, in the case of the trans−trans isomer, crowding of the inner hydrogen atoms) all of these annulenes exist in nonplanar conformations and are thus olefinic. To arrive at planar or near-planar 10-membered rings, two concepts have been applied: (1) replacement of 1,6- or 1,5-positioned hydrogen atoms of [10]annulenes by a CH_2 group affording bridged [10]annulenes[20−26] and (2) introduction of two triple bonds to give 1,6-didehydro[10]annulene.[27] Research on [10]annulenes has focused on 1,6-methano[10]annulene, **1** (see Figure 1), since it is accessible fairly readily, possesses a near-planar C_{10}-perimeter, and is a stable aromatic molecule. Remarkably, only small energy differences[28−31] separate **1** from the norcaradiene-type **2** and olefinic **3** structures (see Figure 1), as evidenced by the finding that substituent effects suffice to convert bridged [10]annulenes into the **2** and **3** forms.[32,33] However, the question as to whether **1**−**3** are local minima or not of the potential energy surface of 1,6-methano[10]annulene in the ground state remains open. Clearly, this intriguing fact has to be taken into account in investigations on 1,6-methano[10]annulene, such as the present spectral study.

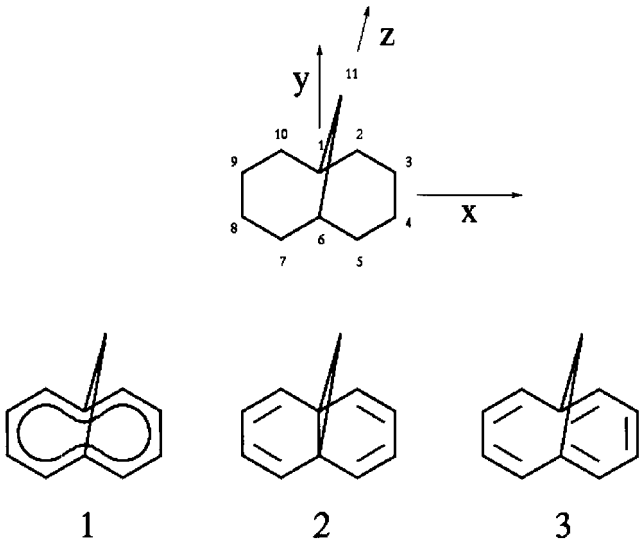

Figure 1. (Top) Atomic numbering of 1,6-methano[10]annulene and molecular reference system. (Bottom) Structures of 1,6-methano-[10]annulene: (1) aromatic, (2) norcaradiene-type, (3) olefinic (or polyenic).

The one-photon UV absorption and MCD spectra of 1,6-methano[10]annulene at room temperature conform to the aromatic behavior, showing four distinct transitions of L_b, L_a, B_b, and B_a parentage, the third and the fourth partially overlapping.[34−38] In this paper we report on fluorescence and fluorescence excitation spectra, $S_0 \leftarrow\rightarrow S_1$, of 1,6-methano-[10]annulene at low temperature in glassy matrixes measured by means of site selection technique,[39] applied with success to molecules of medium/large dimensions.[40−42] The fluorescence spectra, exciting into the $S_0 \rightarrow S_1$ absorption region, and the fluorescence excitation spectra, detected within a sufficiently narrow emission window, show well-resolved vibronic struc-

S1089-5647(98)00161-8 CCC: $15.00
Published on Web 02/24/1998

tures. For both types of experiment photoselection data are helpful for assignment.

Coupled with the experimental study, ab initio MO calculations have been performed for the ground and the first excited electronic state. Similar calculations at the SCF level of theory were already reported,[28−31] mostly dealing with the valence tautomerism of the hydrocarbon in the ground state. No ab initio study has addressed, to our knowledge, the issue of structural and dynamical informations on S_1. By means of density functional (DF)[9,44] and multiconfigurational (MCSCF/CAS)[45,46] calculations and using the 6-31G basis set, the stable, i.e., corresponding to all real vibrational frequencies, S_0 and S_1 equilibrium structures of 1,6-methano[10]annulene have been determined. The $S_0 \leftarrow\rightarrow S_1$ Franck−Condon factors, related to the experimental intensity profiles, have been calculated according to known theoretical models.[47,48]

The paper is organized as follows. After the Experimental Section, the fluorescence and excitation spectra are discussed in section III. Reference will be made in particular to band structures associated with site selection. The results of calculations are presented in section IV. Equilibrium geometries and vibrational frequencies have been calculated for the S_0 and S_1 states and used for Franck−Condon analysis in section V. A short conclusive section summarizes the essential points of our work.

II. Experimental Section

The synthesis of 1,6-methano[10]annulene has been described elsewhere.[20] The sample purity was checked by gas chromatographic and mass analysis. The one-photon absorption and fluorescence spectra of 1,6-methano[10]annulene at room temperature, taken routinely at the start of each experiment, do not show appreciable changes with time and are quite similar to those reported.[34,49] Despite its stability, the material was kept under nitrogen and at ≈0 °C after that small amounts of sample were periodically transferred for the preparation of solutions in isopentane/diethyl ether (7:3) mixtures or, less frequently, in *n*-heptane. The solute concentration was set to $\approx 10^{-3}$ M.

Rigid glassy isopentane/ether matrixes are formed introducing directly into liquid nitrogen the sample cell, previously evacuated from air by several thaw-and-freeze cycles with a diffusion pump. Fluorescence spectra of solid transparent samples may be taken by exciting into the electronic origin or into the vibronic lines of the $S_0 \rightarrow S_1$ transition, without being much affected by scattered incident intensity. In addition, excitation spectra may be measured moving the fluorescence window close to the (0−0) band. As to the absorption spectra, the beam is only slightly attenuated going through the glassy matrix in the absence of absorption, in contrast with the spectral response from polycrystalline samples, and as a consequence, the full dynamic range of the instrumental sensitivity may be exploited. Similar experiments were performed at 15 K, condensing the solution either as a small drop on the cold tip of a closed-circuit He cryostat or in a quartz cell in thermal contact with the tip. A limited series of measurements were carried out at 15 K dissolving 1,6-methano[10]annulene in an *n*-heptane matrix grown slowly from liquid.

The experimental apparatus has been described in a previous paper.[50] Briefly, fluorescence spectra have been measured exciting with the third ($\lambda = 355$ nm) and the fourth ($\lambda = 266$ nm) harmonic of a Nd:YAG laser (Quanta-Ray, model DCR-10), with the fundamental ($\lambda = 337$ nm) of a N_2 laser (Lambda Physik, model EMG-101) and in the range 365−400 nm using a N_2-pumped dye laser equipped with dyes such as EXALITE 384, BBQ, α-NPO, PBBD, and BPBD. The emission signal, dispersed through a Jobin-Yvon double monochromator, is detected by an air-cooled photomultiplier and averaged by the Boxcar (PAR, model 162). The fluorescence spectrum is normalized with respect to the incident intensity, diverting a small portion of the incoming beam to a photodiode by means of a beam splitter. The slit width of the monochromator was ≈200 μm, corresponding to a bandwidth of ≈5 cm^{-1}. The same apparatus was used for excitation spectra, taking as fixed the emission and tuning the laser wavelength. The instrumental bandwidth was ≈5 cm^{-1} for all dyes.

By inserting polarizing optics along the incidence and the emission directions, the fluorescence and excitation polarization ratios were determined.[51] Depending upon the relative orientation of the polarizing optics, two types of experiments are performed, with both incident and emitting radiation vertically polarized or with the latter in crossed polarization with respect to the former. $I_V^{\parallel}$ and $I_V^{\perp}$ are measured in the two cases. The polarization ratio is defined as $(I_V^{\parallel} - I_V^{\perp})/(I_V^{\parallel} + I_V^{\perp})$. A scrambler in front of the monochromator eliminates the instrumental factor favoring the parallel polarization due to the holographic gratings of the monochromator. Other possible sources of error are taken into account by repeating the two experiments with horizontally polarized exciting light. According to theory,[51] $I_H^{\parallel}$ and $I_H^{\perp}$ must be equal. The deviation from unity is the correction factor of the polarization ratio. Absorption spectra of 1,6-methano[10]annulene solutions at room and low temperature were measured on a Cary 5 spectrophotometer with a spectral resolution of ≈20 cm^{-1}.

III. $S_0 \leftarrow\rightarrow S_1$ Transition

Previous studies[34−38] on the electronic spectrum of 1,6-methano[10]annulene have correlated the lowest transition, $S_0 \rightarrow S_1$, to the aromatic L_b transition, with the moment along the *x* axis (see Figure 1 for the molecular reference system). The S_1 state has been described predominantly in terms of |HOMO, LUMO+1⟩ and |HOMO−1, LUMO⟩ excited configurations.[35,38] In this work fluorescence and excitation $S_0 \leftarrow\rightarrow S_1$ spectra have been measured at low temperature as a function of the exciting wavelength and emission window, respectively. They will be considered separately in the next subsections. For a better understanding of our results also the absorption spectrum must be taken into account.

A. One-Photon Absorption and Fluorescence Transitions. The low-temperature fluorescence spectra with $\lambda_{exc} = 355$, 337, and 266 nm have similar structures. Beyond the origin peak (25 081 cm^{-1}, $\lambda_{exc} = 355$, 266 nm; 25 075 cm^{-1}, $\lambda_{exc} = 337$ nm) the band intensity steeply increases and shows a maximum ≈1500 cm^{-1} from the origin and enhanced diffuseness to lower energies. For comparison, the absorption and fluorescence ($\lambda_{exc} = 355$ nm) spectra of 10^{-3} M 1,6-methano[10]annulene in a isopentane/ether solution at 15 K are reported in Figure 2. The fluorescence polarization ratio using the same excitation wavelength is also displayed on top of the corresponding spectrum.

The observed origin peaks, 25 086 (absorption) and 25 081 cm^{-1} (fluorescence, $\lambda_{exc} = 355$ nm), respectively, agree reasonably well with each other, showing that the same transition is responsible for the onset of the two processes. The fluorescence polarization ratio is almost constant, ≈0.25, in the emission range, except in the origin region (≈0.35). Moving the excitation wavelength ($\lambda_{exc} = 383.8$ nm), the ratio shifts almost uniformly to higher values, being ≈0.5 around the (0−0) band. The ratio was found to be 0.4 in a past report.[35] It is therefore concluded that all the fluorescence bands have the same

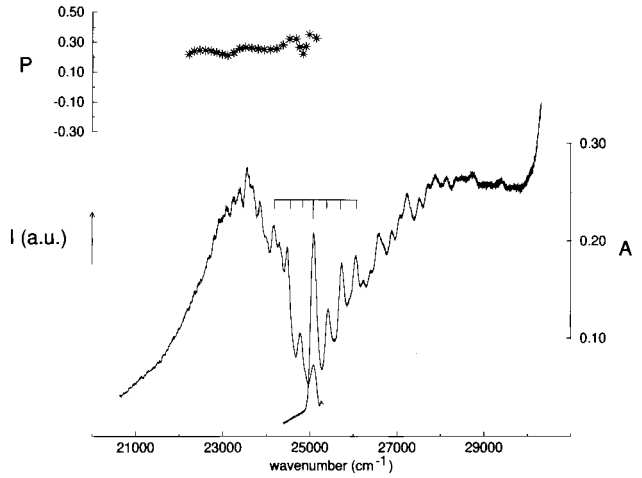

Figure 2. Fluorescence (left; $\lambda_{exc} = 355$ nm) and absorption (right) spectrum of 1,6-methano[10]annulene in isopentane/ether solution ($c = 10^{-3}$ M) at 15 K. The polarization ratio P is shown on top of the fluorescence spectrum. The lowest absorption (335, 649, 971 cm^{-1}) and fluorescence (310, 601, 909 cm^{-1}) vibronic bands are indicated.

emission direction, and the spectrum must essentially be assigned to allowed transitions.

When the two spectra are compared, it is seen that the energy spacings from (0−0) do not match well with each other. The three most prominent absorption bands occur at 335, 649, and 971 cm^{-1}, while the fluorescence counterparts are observed at 310, 601, and 909 cm^{-1}. This suggests that the potential wells of S_0 and S_1 around the minima have appreciably different shapes. Also, spectral intensities change in the two spectra. The fluorescence bands following (0−0) are stronger than the origin, while the reverse is true for absorption. This may be due, at least in part, to the dependence of the fluorescence spectrum on the excitation wavelength. As seen in the following subsection, shifting the excitation wavelength toward (0−0) results in reducing the intensity differences among fluorescence bands. In addition, reabsorption of the (0−0) emission may occur, though difficult to estimate quantitatively. It should also be recalled that in aromatic molecules constructive−destructive interference of allowed and vibronically induced contributions to the transition moment, the latter arising from coupling of electronic states of equal symmetry, may cause asymmetries between the two intensity profiles.[52] In our case, however, the vibronic contribution is expected to be relatively small, given the energy gap, ≈12 000 cm^{-1}, between the *x*-polarized L_b and B_b states in 1,6-methano[10]annulene.[34,35,38] The loss of mirror symmetry is also related to the rotation of normal modes (Duschinsky effect) going from the ground to the excited state.

Finally, it is seen that the fluorescence spectrum has decreasing intensity beyond ≈1500 cm^{-1} from the origin, while the absorption profile steadily increases. This may be evidence of a second, weakly absorbing, electronic state hidden under the $S_0 \rightarrow S_1$ profile. Conclusive evidence on this point comes from two-photon spectroscopy.[38]

B. Site Selection Fluorescence Spectra. Exciting at approximately the lowest absorption maxima (26 055, 25 760, 25 425, and 25 094 cm^{-1}), remarkably sharp fluorescence spectra are observed, as shown in Figure 3. This is related to the selective excitation of a portion of molecules among all those contributing to the absorption band. As noted in the Introduction, the effect has been extensively discussed[39] and applied to complex molecules in rigid solutions.[40−42] Due to the random orientation of molecules in the glassy matrix, absorption bands are inhomogeneously broadened and, in particular, the low-

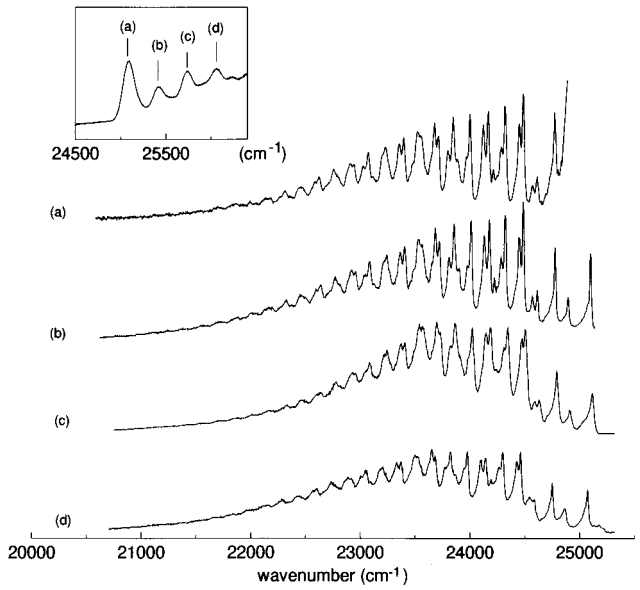

Figure 3. Fluorescence spectra of 1,6-methano[10]annulene in isopentane/ether solution ($c = 10^{-3}$ M) at 15 K, exciting into the $S_0 \rightarrow S_1$ absorption region, as shown in the inset. The excitation energies are (a) 25 094, (b) 25 425, (c) 25 760, and (d) 26 055 cm^{-1}.

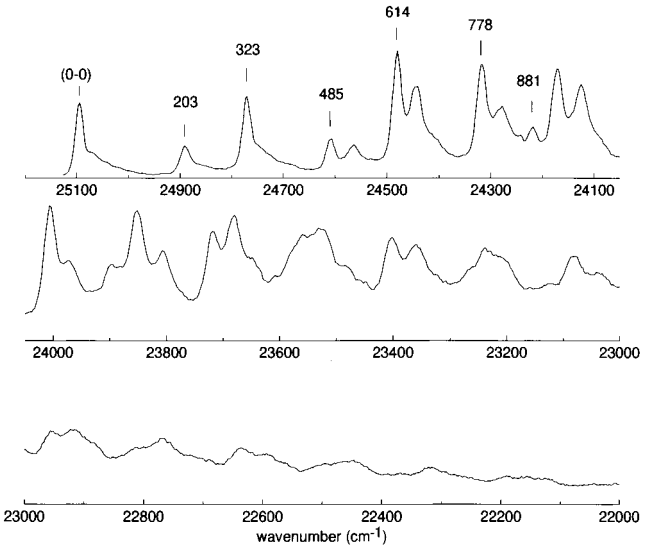

Figure 4. Fluorescence spectrum ($\omega_{exc} = 25\,425$ cm^{-1}) of 1,6-methano[10]annulene in isopentane/ether solution ($c = 10^{-3}$ M) at 15 K. The electronic origin and the frequencies (cm^{-1}) of the most active fundamentals are also shown.

energy bands of Figure 2 have a full width ≈ 180−190 cm^{-1}, independent of the temperature below 77 K. If the excitation line has a narrower width, only a fraction of molecules will be excited, in relation to the absorption coefficient at the incident frequency, and will be responsible for fluorescence. At low concentration, each solute molecule behaves as an impurity inside the glassy matrix, and the fluorescence consists of sharp lines (zero-phonon lines, ZPL), each of them associated with a phonon wing (PW) with relative intensity, I_{PW}/I_{ZPL}, depending on the interaction between the impurity emitting level and the matrix lattice phonons.[39]

Near-UV dye lasers provide excellent excitation sources for site selection studies of 1,6-methano[10]annulene even with a relatively large excitation width (≈5 cm^{-1}, our experimental apparatus). The absolute frequencies of the fluorescence bands change with the incident frequency, as they depend on the molecular subgroup excited within the inhomogeneous profile.

TABLE 1: Excitation (λ_{em} = 403.7 nm) and Fluorescence (λ_{exc} = 393.3 nm) Spectra of 1,6-Methano[10]annulene at 15 K in Isopentane/Ether Solution ($c = 10^{-3}$ M): Observed Frequencies Relative to Origin ($\Delta\omega$, cm^{-1}), Relative Intensities (I), and Proposed Assignment

excitation spectrum origin at 25 090 cm^{-1}			fluorescence spectrum origin at 25 094 cm^{-1}		
$\Delta\omega$	I[a]	ass[b]	$-\Delta\omega$	I[a]	ass[b]
170	w	fund	203	w	fund
332	m	fund	323	s	fund
			408	br	2*203(2)
487	mw	fund	485	mw	fund
			530	w	203+323(4)
			614	s	fund
646	s	fund	650	s	2*323(4)
			778	s	fund
829	mw	332+487(10) 646+170(13)	816	m	614+203(−1);323+485(8)
			852	sh	2*323+203(3)
			881	w	fund
			931	s	614+323(−6)
981	m	332+646(3)	974	s	778+203(−7);3*323(5)
			1096	s	778+323(−5)
1147	m	646+170+332(−1) 487+646(14)?	1128	mw	2*323+485(−3);614+203+323(−11)
			1205	w	881+323(1)
			1248	ms	614+2*323(−12);2*614(20)?
1317	w	fund 2*646(*25)?	1293	mw	4*323(1)
1388	w	fund	1381	mw	778+614(−11);fund?
			1417	mw	778+2*323(−7)
			1451	sh	485+3*323(−3)
1485	mw	fund 646+829(10)?	1493	vw	203+4*323(−2)
			1520	sh	881+2*323(−7)
			1543	m	2*778(−13);2*614+323(−8)
			1573	m	614+3*323(−10)
1620	w	332+2*646(−4)	1617	sh	5*323(2)
			1700	mw	778+614+323(−15)
			1741	mw	778+3*323(−6)
1775	w	487+2*646(−4)			
			1841	sh	3*614(−1);881+3*323(−9)
			1863	mw	2*614+2*323(−11);778+614+485(−14)
			1887	mw	2*778+323(8)
1947	w	1317+646(−16) 3*646(11)?			
			1981	vw	881+323+778(−1)
			2021	w	778+2*614(15);778+614+2*323(−17)
			2064	w	778+4*323(−6)
2103	w	487+332+2*646(−8)			
			2143	w	323+3*614(−22)
			2183	w	2*614+3*323(−14)
			2292	sh	881+778+2*323(−13)
			2331	w	3*778(−3)
			2382	sh	778+5*323(−11)
2386	w	1388+332+646(17)?			
			2465	w	2*323+3*614(−23)
			2506	w	2*614+4*323(−14)
			2605	sh	881+778+3*323(−23)
			2651	w	3*778+323(−3)
			2781	vw	2*778+2*614(−3)
			2912	vw	881+778+614+2*323(−7)
			2976	vw	3*778+2*323(−4)

[a] Relative intensities are indicated as s (strong), m (medium), w (weak), sh (shoulder), br (broad). [b] Values in parentheses are differences between observed and calculated frequencies.

On the contrary, energy differences with respect to the band origin do not show significant variations with the excitation frequency. Due to site selection, the origin band (λ_{exc} = 393.3 nm) has a ZPL width of ≈23 cm^{-1} and a clear phonon wing. Increasing the excitation energy, the band broadens considerably due to loss of site selectivity, and the width approaches that measured in absorption.

Let us now consider in more detail the fluorescence spectrum obtained with λ_{exc} = 393.3 nm (i.e., exciting on the first vibronic band; see inset of Figure 3), shown on an expanded view in Figure 4. The observed frequencies are reported in Table 1. A major difference with the fluorescence spectrum of Figure 2 is the appearance of doublets, ≈35−40 cm^{-1} apart, instead of single broader bands. Following the intense vibronic 323 cm^{-1} peak, a first doublet is observed 614/650 cm^{-1}, a second 778/816 cm^{-1}, and a third 931/974 cm^{-1} from the origin (25 094 cm^{-1}). The effect does not depend on the type of solvent used in this work since the doublets are well-developed also for an *n*-heptane matrix. It has been reported[39] that multiplet band structures are observed upon excitation of molecular subgroups

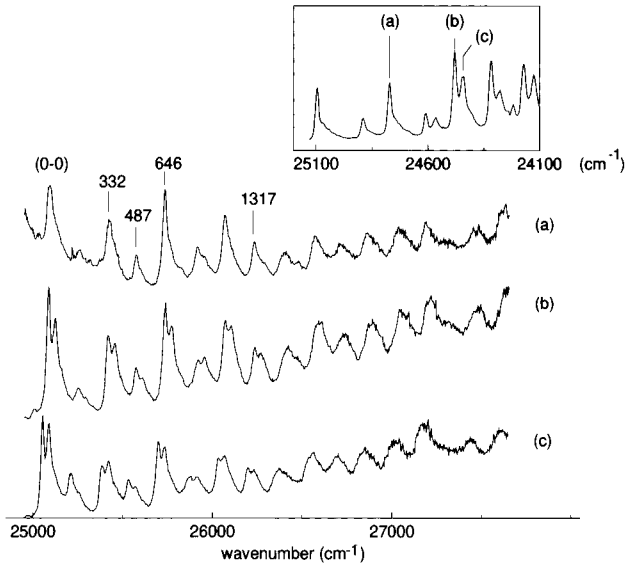

Figure 5. Fluorescence excitation spectra of 1,6-methano[10]annulene in isopentane/ether solution ($c = 10^{-3}$ M) at 15 K as a function of the energy of the fluorescence window, as shown in the inset. The electronic origin and the frequencies (cm^{-1}) of the most active fundamentals are also shown in spectrum a.

belonging to different overlapping bands.[39] These are most clearly seen in the origin region.[40] On the contrary, we observe a single (0−0) band, for all four excitation wavelengths (see Figure 3). On the other hand, infrared and Raman spectra of crystalline 1,6-methano[10]annulene at room temperature show strong vibrational activity for modes occurring at 320, 600, and 763 cm^{-1}.[54] This gives a clue for the assignment: once account is taken of the molecule-to-crystal frequency shift, the spectrum is interpreted as due to progressions of totally symmetric 323, 614, and 778 cm^{-1} fundamentals on several band heads. These fall at 203(w), 323(s), 485(w), 614(s), 778(s), and 881(w) cm^{-1} from the origin. The assignment is summarized in Table 1.

C. One-Photon Fluorescence Excitation Spectra. For dilute samples and narrow-band detection windows the excitation spectrum obtained with tunable dye lasers has a fine structure comparable to that of site-selected fluorescence.[40] We have measured excitation spectra in the 25 000−27 500-cm^{-1} range at 15 K with an emission window on the 323-cm^{-1} peak and on each component of the most prominent doublets. The three spectra measured as shown in the inset are reported in Figure 5. The excitation spectrum at 77 K and the polarization ratio ($\lambda_{em} = 414.7$ nm, ≈970 cm^{-1} from (0−0), in correspondence with the third doublet of Figure 4) are displayed in Figure 6.

There are several points of comment about these results. These are (1) the spectrum a of Figure 5 ($\lambda_{em} = 403.7$ nm) consists of sharp single bands. The strongest absorption bands have, within experimental accuracy, excitation counterparts. Additional excitation bands are observed, weakly appearing or absent in the absorption spectrum; (2) placing the emission window at 408.5 and 409.1 nm (i.e., in correspondence with the first fluorescence doublet), doublets are observed in the excitation spectra b and c. The spectral structure is seen also with emission windows on other doublets; (3) the excitation polarization ratio changes as a function of energy, in contrast with the fluorescence ratio. Minima (≈0.3) are found around 500, 820, and 1110 cm^{-1} from (0−0). The ratio slowly decreases on going to higher energies.

The observed excitation frequencies and the proposed assignment, based on the comparison with fluorescence data, are collected in Table 1. The strongest band, 646 cm^{-1}, has been

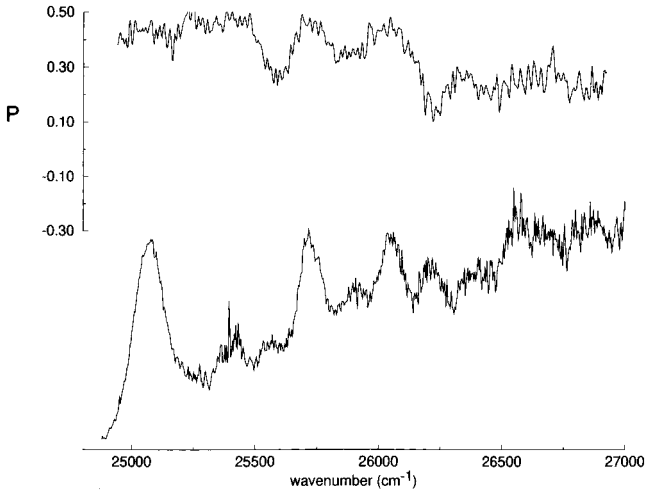

Figure 6. Fluorescence excitation spectrum and polarization ratio of 1,6-methano[10]annulene in isopentane/ether solution ($c = 10^{-3}$ M) at 77 K.

correlated with the most intense fluorescence band, 614 cm^{-1}. A moderate (or small) frequency increase is found for the other two low-frequency modes, 323/485 cm^{-1} in S_0 and 332/487 cm^{-1} in S_1. The 203 cm^{-1} fluorescence mode decreases to 170 cm^{-1} in the excited state. More interesting, no excitation band is observed in correspondence with the 778 cm^{-1} fluorescence peak, and overtones of the 332 cm^{-1} band are absent (or too weak to be observed). These qualitative findings are fairly well-described by frequency and intensity calculations relative to the S_0 and S_1 states of section V.

As to the appearance of doublets in the excitation spectra, it should be noted that their splitting, ≈35 cm^{-1}, is equal to that found for fluorescence doublets (see Figure 4). As already pointed out in the last subsection, multiplet structures have been observed in site-selected fluorescence spectra and related to the occurrence of excited vibronic levels with an energy difference smaller than the inhomogeneous width.[40] This may be repeated in our case, simply substituting ground- for excited-state levels. The situation is qualitatively sketched in Figure 7 .[39] As the excitation beam, ω_{ex}, sweeps across the inhomogeneous profile, a single band is observed in the spectrum when the (fixed) emission frequency, ω_{em}, is equal to the frequency of a fluorescence band (intermediate point, Figure 7a). If two bands are within the inhomogeneous width, the previous condition may be satisfied twice, and a doublet is observed (second and third point, Figure 7b). Therefore, the two series of bands in spectra b and c of Figure 5 have vibronic intervals with respect to the respective origin equal to those of the upper spectrum (a).

On the basis of the excitation results, the origin and the strongest vibronic bands (332, 646, and 981 cm^{-1}) have the same absorption direction, i.e., along the *x* axis. Therefore, these modes are totally symmetric. In contrast, the 500, 820, and 1110 cm^{-1} minima, though not equal to −1/3, are assigned to weak vibronic transitions with the absorption direction perpendicular to *x*, i.e., along either the *y* or *z* axis. The vibrational modes are non totally symmetric. Similar results have been already reported.[34,35] According to these data, the excitation spectrum has allowed and weak vibronically induced contributions to the intensity. The latter is associated with the 500, 820, and 1110 cm^{-1} minima. Plausibly, a progression is built on the 500 cm^{-1} mode involving the 332 and 646 cm^{-1} modes.

IV. S_0 and S_1 States: Results of Calculation

In the past years several ab initio calculations have been carried out on the electronic ground state of 1,6-methano-

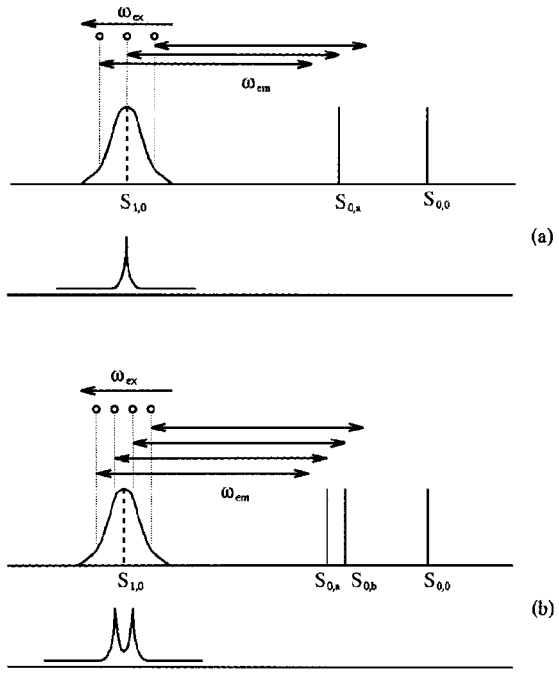

Figure 7. Occurrence of a singlet (upper, a) and a doublet (lower, b) band structure in the excitation spectrum of a molecule in rigid solution. $S_{0,0}$ is the vibrationless ($v = 0$) electronic ground state; $S_{1,0}$ is the inhomogeneously broadened vibrationless ($v = 0$) first excited state; $S_{0,a}$, $S_{0,b}$ are excited vibrational levels of the ground state; ω_{exc} is the tunable excitation energy; ω_{em} is the fixed emission energy.

TABLE 2: Restricted Hartree−Fock (RHF) Energies (au), without and with MP2 Contribution, of the Three Structures 1−3 (See Figure 1) Corresponding to the SCF Optimized Geometries as a Function of the Basis Set

	1	**2**	**3**
6-31G	−422.135 220	−422.126 512	−422.135 259
6-31G+MP2	−423.114 693	−423.089 848	−423.113 214
6-31G**	−422.303 777	−422.304 620	−422.304 508
6-31G**+MP2	−423.788 751	−423.764 167	−423.779 987
DZV	−422.167 316	−422.158 436	−422.167 392
DZV+MP2	−423.098 585	−423.072 648	−423.096 532
DZV**	−422.359 259	−422.360 185	−422.360 020
DZV**+MP2	−423.815 574	−423.790 094	−423.806 655

[10]annulene.[28,30,31] Three different extrema were determined using the 6-31G basis set,[31] corresponding to the aromatic, norcaradiene-type, and olefinic (or polyenic) structures **1**−**3** of Figure 1. The structure **3** may occur in two equivalent configurations, interconverted by a π bond shift, as observed in the case of tetrakis(trimethylsilyl)-1,6-methano[10]annulene.[32]

In a first step we have repeated these calculations with the GAMESS program[55] extending the basis set (6-31G, 6-31G**, DZV, DZV**). The energies of **1**−**3** at the appropriate equilibrium geometries decrease moderately on changing the basis set, as shown in Table 2. The structure **1** (or "aromatic") does not correspond to the lowest energy. The isomer **2** (or "norcaradiene-type") has the lowest energy with the polarized sets, while the "polyenic" form **3**, with the 6-31G and DZV sets. However, in the latter two cases the energy differences with the "aromatic" isomer are too small to be significant. The calculated structure of **1** at the 6-31G level is in excellent agreement with experimental data,[56,57] as already noted.[31] The effect of basis change on the structural parameters of this as well as of **2** and **3** is minor. The results for **1** are reported in Table 3.

The three extrema may correspond or not to minima of 1,6-methano[10]annulene in the ground state. To this purpose, the

TABLE 3: Experimental and Calculated C−C Bond Lengths (Å) of the Aromatic Isomer 1 of 1,6-Methano[10]annulene. Atom Pairs in the First Column Are Numbered as in Figure 1[a]

	expt[b]		6-31G	6-31G**	DZV	DZV**
C_1-C_2	1.402	1.427	1.406	1.408	1.413	1.415
C_2-C_3	1.378	1.383	1.379	1.374	1.388	1.380
C_3-C_4	1.417	1.416	1.423	1.424	1.431	1.429
C_1-C_{11}	1.484	1.478	1.487	1.481	1.491	1.483
$C_1\cdots C_6$	2.235	2.257	2.244	2.211	2.249	2.217

[a] The distance (Å) between nonbonded 1,6 atoms is also included. [b] From refs 56 and 57.

vibrational frequencies of **1**−**3** must be calculated. If all normal frequencies are real, the structure is stable with respect to any atomic displacement out of the equilibrium configuration and is associated with a minimum on the potential energy surface. It turns out that **2** and **3** have stable equilibrium structures, while the C_{2v} structure **1**, with one b_1 imaginary frequency, 105i cm^{-1}, lies on a saddle point. Allowing the latter to relax along this coordinate, only the *xz* symmetry plane is conserved and the structure changes from **1** to **3**. It is concluded that in the restricted Hartree−Fock (RHF) approximation **1** is the transition state between equivalent **3** configurations. The same conclusion is reached using the other basis sets.

It is however well-known[58−60] that bond-equalized structures such as **1** are preferred at the correlation level of theory. The effect, taken into account through the MP2 correction, reverses the energy ordering between **1** and **3**, favoring the former by ≈400 cm^{-1} (6-31G basis set).[31] This order is maintained on increasing the basis size, as seen in Table 2. The norcaradiene-type isomer lies higher, ≈5500 cm^{-1}, and the polyenic form **3** in intermediate position, ≈400 cm^{-1} without and ≈1900 cm^{-1} with polarization functions. Unfortunately, with our present GAMESS resources it is not possible to find minima at the MP2 level and to perform the vibrational analysis of **1**−**3**. Alternatively, we have carried out additional calculations on the three isomers with the density functional (DF) formalism using the GAUSSIAN 94 program.[61] Full account of these calculations will be reported elsewhere.[54] According to our DF data, the ground-state energy surface has only one minimum, corresponding to isomer **1**. It may be seen from Table 4 that with the 6-31G basis set and the B3-LYP functional[9,44] all normal modes of **1** (including those of b_1 symmetry) have real frequencies. On the contrary, the bond alternating structures **2** and **3** are no longer equilibrium configurations, smoothly converging to **1** during the structure optimization process.

The geometry and energy of the lowest, S_1, excited state have been calculated by means of the MCSCF/CAS wave function, including all possible promotions of 10 electrons among the 10 MOs with the largest p_z contribution from perimetric C atoms. Because of the nonplanarity of the cycle, each molecular orbital has in principle nonvanishing contributions from all atomic orbitals, and strictly speaking, the classification into π and π^* MOs has no meaning. Although at the SCF level of theory the molecular orbitals are different for the three isomers, the MCSCF/CAS calculation for S_1 gives the same C_{2v} structure, with reduced bond alternancy along the cycle and increased 1,6 interannular distance with respect to S_0. The S_1 energy and C−C bond lengths are reported in Table 5. The S_1 structure corresponds to a minimum of the potential energy surface, as shown by the fact that all the associated frequencies are real (see Table 5). Repeating the MCSCF/CAS calculation for S_0 (aromatic form) an energy value of −422.271 301 au is obtained. The aromatic structure corresponds, as in previous RHF

TABLE 4: Energy (*E*, au), C−C Bond Lengths (Å), and Vibrational Frequencies (cm^{-1}) of the Ground State of 1,6-Methano[10]annulene, According to DF Calculations with the B3-LYP Functional and Using the 6-31G Basis Set. Atom Pairs in the First Column Are Numbered as in Figure 1;[a] A_1, b_1, and b_2 Modes Are Directed along the *z*, *x*, and *y* Axes, Respectively, As Defined in Figure 1

E		−425.029 428	
C_1-C_2		1.413	
C_2-C_3		1.398	
C_3-C_4		1.429	
C_1-C_{11}		1.500	
$C_1\cdots C_6$		2.308	
a_1 198	b_1 315	a_2 179	b_2 354
344	441	387	469
501	685	631	657
649	722	830	790
793	899	913	883
906	964	1012	967
954	1055	1143	1015
1003	1254	1229	1180
1260	1329	1325	1337
1402	1408	1526	1359
1499	1582	1643	1469
1539	3153	3151	1600
1548	3159	3171	3152
3093	3184		3173
3161			
3186			

[a] The distance (Å) between nonbonded 1,6 atoms is also included.

TABLE 5: Energy (*E*, au), C−C Bond Lengths (Å), and Vibrational Frequencies (cm^{-1}) of 1,6-Methano[10]annulene in the First Excited State S_1 According to MCSCF/CAS Calculations and Using the 6-31G Basis Set. Atom Pairs in the First Column Are Numbered as in Figure 1;[a] A_1, b_1, and b_2 Modes Are Directed along the *z*, *x*, and *y* Axes, Respectively, as Defined in Figure 1

E		−422.164 878	
C_1-C_2		1.422	
C_2-C_3		1.424	
C_3-C_4		1.432	
C_1-C_{11}		1.500	
$C_1\cdots C_6$		2.424	
a_1 186	b_1 390	a_2 161	b_2 352
354	443	387	385
506	692	539	541
700	715	782	793
720	890	940	810
869	952	967	940
929	1123	1133	1004
998	1311	1299	1189
1315	1374	1405	1424
1479	1592	1593	1460
1577	1975	1714	1544
1631	3281	3314	1607
1680	3321	3332	3315
3237	3348		3334
3324			
3349			

[a] The distance (Å) between nonbonded 1,6 atoms is also included.

calculations, to a saddle point with one low imaginary frequency of b_1 symmetry. The energy difference $\Delta E(S_1 - S_0)$, ≈23 360 cm^{-1}, is however in reasonable agreement with the experimental data. The S_1 wave function is mostly described in terms of only two singly excited configurations, i.e., $\psi(S_1) \approx -0.5|\text{HOMO}-1, \text{LUMO}\rangle + 0.6|\text{HOMO}, \text{LUMO}+1\rangle$ and has B_1 symmetry. These are also the most important excited configurations found with semiempirical methods.[35,38] The S_0 → S_1 oscillator strength is calculated to be 0.0009 as compared with the experimental value of 0.003.[34]

TABLE 6: Calculated Vibronic Intensities Relative to the (0−0) Intensity (I/I_0) of the Totally Symmetric Modes (ω, cm^{-1}): Left, $S_0 \rightarrow S_1$ Transitions; Right, $S_1 \rightarrow S_0$ Transitions

$S_0 \rightarrow S_1$		$S_1 \rightarrow S_0$	
ω	I/I_0	ω	I/I_0
186	0.008	203	0.002
354	0.282	358	0.548
506	0.013	514	0.001
700	1.205	656	0.805
720	0.258	805	0.269
869	0.044	935	0.006
929	0.120	964	0.072
998	0.123	1041	0.002
1315	0.002	1335	0.012
1479	0.008	1470	0.001
1577	0.033	1566	0.033
1631	0.048	1625	0.007
1680	0.002	1669	0.001

V. Discussion

According to our DF and MCSCF/CAS calculations, only the isomer **1** is stable in the ground and in the first excited state. The observed fluorescence and fluorescence excitation spectra are therefore assigned to this isomer.

Neglecting in a first approximation frequency differences between the ground (g) and excited (e) state vibrational modes, the transition strength of allowed vibronic bands, $S_{0,0} \rightarrow S_{1,\upsilon}$ and $S_{1,0} \rightarrow S_{0,\upsilon}$, can be calculated on the basis of the Franck−Condon principle by means of the adimensional displacement factor B given by[47]

$$B = (4\pi^2 c\omega/h)^{1/2}\Delta Q \qquad (1)$$

where $\omega = \omega_e = \omega_g$ is the vibrational frequency (cm^{-1}) and ΔQ is the difference between normal coordinates at equilibrium in the excited and ground electronic state. The $0-\upsilon$ transition has intensity with respect to that of the origin given by[48]

$$I_{0,\upsilon}/I_{0,0} = (0.5B^2)^{\upsilon}/(\upsilon)! \qquad (2)$$

where υ is the excited vibrational level of a totally symmetric mode Q. The ΔQ difference may be expressed in terms of the Cartesian displacement column vector L (of $3n$ components) of the Q mode and of the geometry change between ground and excited state so that B results in

$$B = 0.172\omega^{1/2}(\mathbf{X_1} - \mathbf{X_0})m^{1/2}L \qquad (3)$$

where $\mathbf{X_1}$ and $\mathbf{X_0}$ are row vectors consisting of the equilibrium $3n$ Cartesian coordinates of the first excited and ground state, respectively, and $m^{1/2}$ is the diagonal ($3n \times 3n$) square root matrix of the atomic masses. The numerical factor appearing in eq 3 results from the expression $[4\pi^2 c/(hN)]^{1/2} \times 10^{-8}$ (allowing also the conversion from $uma^{1/2}$ Å to $g^{1/2}$ cm) and has units $g^{-1/2}$ $cm^{-1/2}$. For reasons of internal consistency of the calculation the Cartesian vectors L of the totally symmetric modes in the ground state have been obtained following the same MCSCF/CAS procedure applied to the calculation of excited-state modes. These a_1 frequencies (see Tables 4 and 6) as well as the equilibrium structure compare reasonably well with results from the DF calculation. Since the $\mathbf{X_1}$ and $\mathbf{X_0}$ quantities as well as the Cartesian displacement vectors of the aromatic isomer for the two states are known, Franck−Condon factors have been calculated, according to eqs 1−3, for all totally

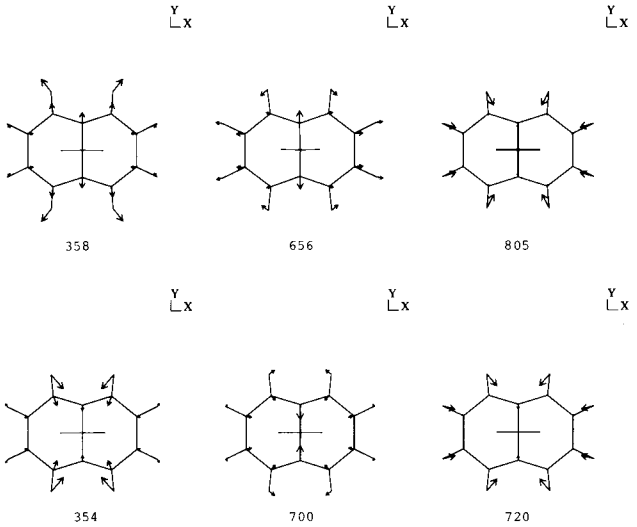

Figure 8. Most active totally symmetric vibrational modes in the fluorescence (upper) and excitation (lower) spectra. Frequency values are in cm^{-1}.

symmetric fundamental ($v = 1$) modes, except C−H stretchings. Fluorescence and absorption intensities include approximately the Duschinsky rotation of normal modes, when ground-state (for fluorescence) and excited-state (for excitation) vibrational displacements are used.[62] The results are collected in Table 6.

The most active modes are calculated at 700 cm^{-1} (exc) and at 656 cm^{-1} (fluor) and are therefore correlated to the 646 cm^{-1} excitation and to the 614 cm^{-1} fluorescence peak, respectively. Among other excitation modes, the second and third most intense are calculated at 354 cm^{-1} (332 cm^{-1}, obs) and 720 cm^{-1}, while all other modes with frequency above 800 cm^{-1} have weak (or extremely weak) intensity. Fluorescence intensities change with respect to excitation. The 656 and 358 cm^{-1} modes have more comparable activity. The third largest is associated with the 805 cm^{-1} mode. The calculated factors are correlated with intensities of the 323, 614, and 778 cm^{-1} bands, the latter being however underestimated. Again, all other modes contribute negligibly to the allowed intensity. This gives support to the proposed assignment of the fluorescence spectrum in Table 1. It should be noted that observed frequencies are a factor 0.91−0.95 smaller than calculated. If a reduction factor in the same range is used for the 720 cm^{-1} mode of the excitation spectrum, the band should fall close to the strong 646 cm^{-1} peak. In fact, just above this peak a shoulder is observed, which is tentatively related to the 720 cm^{-1} mode. The most active totally symmetric modes are graphically shown in Figure 8. Considering the atomic displacements, they favor the change of the equilibrium structure from S_0 to S_1 (and vice versa).

As to the vibronically induced portion of the excitation spectrum built on the 500 cm^{-1} band, no quantitative intensity calculation with respect to the allowed contribution has been attempted. We note only that the excited-state 539 and 541 cm^{-1} modes, of a_2 and b_2 symmetry, respectively, are good candidates for assignment. Qualitatively, the first choice is preferred, given that S_1 (L_b) may interact with the relatively strong and close S_2 (L_a) state through a_2 vibrations.

VI. Conclusions

In this paper fluorescence and fluorescence excitation spectra of 1,6-methano[10]annulene have been measured at low temperature as a function of the incident and emission energy, respectively. Spectral properties under site selection conditions have been analyzed to discuss ground- and excited-state potential surfaces.

According to the structural criterion of aromaticity and antiaromaticity,[4] aromatic (antiaromatic) species are characterized by ground-state potential minima of the bond-equalized (bond-alternating) cyclic structure. Benzene and cyclobutadiene are classical examples of the two categories. In the case of 1,6-methano[10]annulene, the molecule in the ground state has aromatic character. Only one stable S_1 state with C_{2v} symmetry is predicted by MCSCF/CAS calculation. The $S_0 \leftarrow\rightarrow S_1$ spectroscopy of 1,6-methano[10]annulene is related to the aromatic isomer.

Application of fluorescence techniques to other large [4*n*+2]-annulenes or to CH_2-substituted methano[10]annulenes would help to assess in more detail the role of molecular flexibility as a factor opposing aromaticity.

Acknowledgment. The authors gratefully thank Prof. E. Vogel for the generous gift of a sample of 1,6-methano[10]-annulene and for constructive suggestions and corrections about the manuscript. This work was supported by the Italian Consiglio Nazionale delle Ricerche (CNR) and Ministero dell'Università e della Ricerca Scientifica e Tecnologica (MURST).

References and Notes

(1) Herzberg, G. *Electronic Spectra of Polyatomic Molecules*; Van Nostrand: New York, 1975.
(2) Ziegler, L. D.; Hudson, B. S. In *Excited states, vol. 5*; Lim, E. C., Ed.; Academic Press: New York, 1982; p 42.
(3) Pariser, R. *J. Chem. Phys.* **1956**, *26*, 250.
(4) Minkin, V. I.; Glukhovtsev, M. N.; Simkin, B. Y. *Aromaticity and Antiaromaticity;* John Wiley and Sons: New York, 1994.
(5) Turro, N. J. *Modern Molecular Photochemistry;* University Science Books: Mill Valley, CA, 1991.
(6) Henry, B. R.; Siebrand, W. M. In *Organic Molecular Photophysiscs, vol. 1;* Birks, J. B., Ed.; Wiley-Interscience: New York, 1973; p 153.
(7) Platt, J. R. *J. Chem. Phys.* **1949**, *17*, 484.
(8) Hopkins, J. B.; Powers, D. E.; Smalley, R. E. *J. Chem. Phys.* **1980**, *72*, 5039.
(9) Beck, S. M.; Hopkins, J. B.; Powers, D. E.; Smalley, R. E. *J. Chem. Phys.* **1981**, *74*, 43.
(10) Gutmann, M.; Schonzart, P. F.; Hohlneicher, G. *Chem. Phys.* **1990**, *140*, 107.
(11) Wolf, J.; Hohlneicher, G. *Chem. Phys.* **1994**, *181*, 185.
(12) Lambert, W. R.; Felker, P. M.; Syage, J. A.; Zewail, A. H. *J. Chem. Phys.* **1984**, *81*, 2195.
(13) Bree, A.; Leyderman, A.; Salvi, P. R.; Taliani, C. *Chem. Phys.* **1986**, *110*, 211.
(14) Orlandi, G.; Palmieri, P.; Tarroni, R.; Zerbetto, F.; Zgierski, M. Z. *J. Chem. Phys.* **1994**, *100*, 2458.
(15) Swiderek, P.; Hohlneicher, G.; Maluendes, S. A.; Dupuis, M. *J. Chem. Phys.* **1993**, *98*, 974.
(16) Zerbetto, F.; Zgierski, M. Z. *Chem. Phys.* **1988**, *127*, 17.
(17) Gruner, D.; Nguyen, A.; Brumer, P. *J. Chem. Phys.* **1994**, *100*, 2458.
(18) Garratt, P. *Aromaticity*; John Wiley and Sons: New York, 1986.
(19) Masamune, S.; Hojo, K.; Hojo, K.; Bigam, G.; Rabenstein, D. L. *J. Am. Chem. Soc.* **1971**, *93*, 4966.
(20) Vogel, E.; Roth, H. D. *Angew. Chem., Int. Ed. Engl.* **1964**, *3*, 228.
(21) Masamune, S.; Brooks, D. W. *Tetrahedron Lett.* **1977**, 3239.
(22) Scott, L. T.; Brunsvold, W. R.; Kirms, M. A.; Erden, I. *Angew. Chem., Int. Ed. Engl.* **1981**, *20*, 274.
(23) Scott, L. T.; Brunsvold, W. R.; Kirms, M. A.; Erden, I. *J. Am. Chem. Soc.* **1981**, *103*, 5216.
(24) Masamune, S.; Brooks, D. W.; Morio, K.; Sobezak, R. L. *J. Am. Chem. Soc.* **1976**, *98*, 8271, 8277.
(25) Gilchrist, T. L.; Tuddenham, D.; McCague, R.; Moody, C. D.; Rees, C. W. *J. Chem. Soc., Chem. Commun.* **1981**, 657.
(26) McCague, R.; Moody, C. D.; Rees, C. W. *J. Chem. Soc., Chem. Commun.* **1982**, 497.
(27) Meyers, A. G.; Finney, N. S. *J. Am. Chem. Soc.* **1992**, *114*, 10986.
(28) Cremer, D.; Dick, B. *Angew. Chem., Int. Ed. Engl.* **1982**, *21*, 865.
(29) Farnell, L.; Kao, J.; Radom, L., H. F. S., III. *J. Am. Chem. Soc.* **1981**, *103*, 2147.

(30) Farnell, L.; Radom, L. *J. Am. Chem. Soc.* **1982**, *104*, 7650.
(31) Haddon, R. C.; Raghavachari, K. *J. Am. Chem. Soc.* **1985**, *107*, 289.
(32) Neidlein, R.; Wirth, W.; Gieren, A.; Lamm, V.; Hubner, T. *Angew. Chem., Int. Ed. Engl.* **1985**, *24*, 587.
(33) Vogel, E.; Scholl, T.; Lex, J.; Hohlneicher, G. *Angew. Chem., Int. Ed. Engl.* **1982**, *21*, 869.
(34) Blattmann, H.-R.; Boll, W. A.; Heilbronner, E.; Hohlneicher, G.; Vogel, E.; Weber, J.-P. *Helv. Chim. Acta* **1966**, *49*, 2017.
(35) Dewey, H. J.; Deger, H.; Frolich, W.; Dick, B.; Klingensmith, K. A.; Hohlneicher, G.; Vogel, E.; Michl, J. *J. Am. Chem. Soc.* **1980**, *102*, 6412.
(36) Briat, B.; Schooley, D. A.; Records, R.; Bunnenberg, E.; Djerassi, C.; Vogel, E. *J. Am. Chem. Soc.* **1968**, *90*, 4691.
(37) Klingensmith, K. A.; Puttmann, W.; Vogel, E.; Michl, J. *J. Am. Chem. Soc.* **1983**, *105*, 3375.
(38) Catani, L.; Gellini, C.; Salvi, P. R.; Marconi, G. *J. Photochem. Photobiol. A* **1997**, *105*, 123.
(39) Personov, R. I. In *Spectroscopy and Excitation Dynamics of Condensed Molecular Crystals*; Agranovich, V. M., Hochstrasser, R. M., Eds.; North-Holland: Amsterdam, 1983; p 555.
(40) Personov, R. I.; Al'shits, E. I.; Bykovskaya, L. A. *Opt. Commun.* **1972**, *6*, 169.
(41) Personov, R. I.; Al'shits, E. I. *Chem. Phys. Lett.* **1975**, *33*, 85.
(42) Bykovskaya, L. A.; Personov, R. I.; Romanovskii, Y. V. *Anal. Chim. Acta* **1981**, *125*, 1.
(43) Becke, A. D. *Phys. Rev. A* **1988**, *33*, 3098.
(44) Lee, C.; Yand, W.; Parr, R. G. *Phys. Rev. B* **1988**, *37*, 785.
(45) Roos, B. O.; Taylor, P. R.; Siegbahn, P. E. *Chem. Phys.* **1980**, *157*, 48.
(46) Matos, J. M. O.; Roos, B. O.; Malmqvist, P. A. *Chem. Phys.* **1980**, *157*, 48.
(47) Siebrand, W. M.; Zgierski, M. Z. In *Excited States, vol. 4*; Lim, E. C., Ed.; Academic Press: New York, 1979; p 2.
(48) Zerbetto, F.; Zgierski, M. Z. *Chem. Phys.* **1986**, *110*, 421.
(49) Perkampus, H.-H. *UV-VIS Atlas of Organic Compunds*; VCH: Weinheim, 1992.
(50) Gellini, C.; Salvi, P. R.; Hafner, K. *J. Phys. Chem.* **1993**, *97*, 8152.
(51) Albrecht, A. *J. Mol. Spectrosc.* **1961**, *6*, 84.
(52) Craig, D. P.; Small, G. J. *J. Chem. Phys.* **1969**, *50*, 3827.
(53) Catani, L. Chemistry Degree, Thesis, University of Florence, 1996.
(54) Salvi, P. R. To be published.
(55) Dupuis, M.; Spangler, D.; Wendoloski, J. J. *NRCC Software Catalog, vol. 1, program n. QG01, GAMESS*; University of California, Berkeley, 1980.
(56) Bianchi, R.; Pilati, T.; Simonetta, M. *Acta Crystallogr.* **1978**, *B34*, 2157.
(57) Coetzer, J. *Diss. Abstr. B* **1969**, *29*, 3671.
(58) Schweig, A.; Thiel, W. *J. Am. Chem. Soc.* **1981**, *103*, 1420.
(59) Jug, K.; Fasold, E. *J. Am. Chem. Soc.* **1987**, *109*, 2263.
(60) Yoshizawa, K.; Kato, T.; Yamabe, T. *J. Phys. Chem.* **1996**, *100*, 5697.
(61) Frisch, M. J.; et al. *Gaussian 94, Revision D.3;* Gaussian Inc.: Pittsburgh, 1995.
(62) Zgierski, M. Z. *Chem. Phys.* **1986**, *108*, 61.